Interactions between halide anions and a molecular hydrophobic interface

Blake M. Rankin, Michael D. Hands, David S. Wilcox, K. Rebecca Fega, Lyudmila V. Slipchenko and Dor Ben-Amotz*

Received 24th April 2012, Accepted 7th June 2012
DOI: 10.1039/c2fd20082a

Interactions between halide ions (fluoride and iodide) and t-butyl alcohol (TBA) dissolved in water are probed using a recently developed hydration-shell spectroscopic technique and theoretical cluster and liquid calculations. High signal-to-noise Raman spectroscopic measurements are combined with multivariate curve resolution (Raman-MCR) to reveal that while there is little interaction between aqueous fluoride ions and TBA, iodide ions break down the tetrahedral hydration-shell structure of TBA and produce a red-shift in its CH stretch frequency, in good agreement with the theoretical effective fragment potential (EFP) molecular dynamics simulations and hybrid quantum/EFP frequency calculations. The results imply that there is a significantly larger probability of finding iodide than fluoride in the first hydration shell of TBA, although the local iodide concentration is apparently not as high as in the surrounding bulk aqueous NaI solution.

1 Introduction

The affinity of ions for aqueous interfaces is at the heart of Hofmeister's original observations of the influence of salts on protein stability.[1,2] However, many fundamental questions remain regarding the interactions between various ions and proteins as well as macroscopic and molecular hydrophobic interfaces. Although it is widely accepted that ions such as Na^+ and F^- (which "salt-out" non-polar solutes) are repelled from hydrophobic interfaces, some experimental and theoretical results suggest that the opposite is the case for large polarizable anions such as I^- and SCN^- (which "salt-in" non-polar solutes). However, substantial questions remain regarding the magnitude of the latter affinity and the distribution of ions with respect to a hydrophobic interface, particularly when the interface is the hydration-shell of a dissolved hydrophobic group. Here we address the latter issue using a recently developed hydration-shell spectroscopic technique,[3–7] combined with effective fragment potential (EFP) molecular dynamics (MD) simulations and hybrid QM/EFP calculations.[8–11]

Previous experiments, including mass spectrometry,[12] X-ray photoelectron and fluorescence spectroscopies,[13,14] and nonlinear optical surface spectroscopies,[15] all suggest that large anions such as I^- have an affinity for air–water interfaces, while small ions such as F^- do not (although some surface tension[16] and gas bubble electrophoretic mobility[17] experiments are apparently inconsistent with that latter conclusion). However, none of the above experiments are able to determine definitively the degree to which I^- has an enhanced likelihood of residing precisely at the interface, as opposed to one or more hydration layers below the surface. Theoretical studies further suggest that the surface affinity of anions in liquid water and

Department of Chemistry, Purdue University, West Lafayette, Indiana, United States

hydrate clusters can be quite sensitive to both ion size[1,12,18–20] and polarizability,[21,22] although the relative importance of ion size and polarizability remains a subject of debate.[23]

Here we focus on experimentally probing the interactions between halide anions and molecular hydrophobic hydration-shells, whose high curvature and structure might influence ion surface affinities. Previous theoretical and experimental studies relevant to this issue have reached mixed conclusions. For example, classical polarizable molecular dynamics simulations have suggested that[22a] "…heavier halides exhibit affinity to the amide group and to non-polar protein patches…resembling their behavior at the air/water interface" while a more recent combined NMR and simulation study of an uncharged elastin-like polypeptide, $(VPGVG)_{120}$, in aqueous NaSCN has refined this notion by showing that,[22b] although SCN^- interacts with backbone CH_n groups, "…hydrophobic side chains do not contribute significantly to anion binding or the corresponding salting-in behavior…".

In order to further investigate the interaction between salts and molecular hydrophobic interfaces we have performed hydration-shell spectroscopic measurements of aqueous salt solutions containing an alcohol, $(CH_3)_3COH$ (t-butyl alcohol, TBA), whose three methyl groups provide a molecular hydrophobic interfaces which we use to probe the interfacial affinity of F^- and I^- ions. Our results reveal clear differences between the influence of F^- and I^- on vibrational spectral features arising from both the CH stretch of TBA and its hydration shell. Although some of our results speak for themselves, we have attempted to further elucidate their structural significance with the aid of both *ab initio* cluster calculations, liquid MD simulations, and hybrid quantum-classical calculations performed using the effective fragment potential (EFP) methodology.[8–11] More specifically, the key question which we aim to address is whether either F^- or I^- significantly populate the first hydration-shell of TBA, and if so, how does the local ion concentration (and angular distribution) compare with that in the surrounding bulk aqueous salt solution?

The remainder of this manuscript is organized as follows. In Section 2 we describe the experimental procedures used to investigate the affinities of ions for the molecular hydrophobic hydration-shell of TBA, as well as the cluster and liquid calculations used to aid and extend the interpretation of our experimental measurements. The results are described and discussed in Section 3, and then summarized in Section 4.

2 Experimental and theoretical methods

A Raman-MCR experiments

The hydration-shell spectroscopic experimental technique employed in the present work combines high signal-to-noise Raman spectra of variable concentration solutions with multivariate curve resolution (Raman-MCR). We have previously demonstrated the capability of this method in detecting H-bonds and pi-H-bonds between water and polar solutes, ions, and aromatics, as well as the presence of dangling OH bonds in the hydration shells of hydrophobic groups.[3–7] In essence, Raman-MCR facilitates the decomposition of two-component solution spectra into pure solvent and solute-correlated (SC) contributions. The resulting SC spectra may contain features arising from both solute intramolecular vibrations and solute-induced perturbations of solvent molecules. Most of the results described in this work have been obtained using an MCR algorithm called self-modeling curve resolution (SMCR),[24] which is an analytical (as opposed to iterative) method for performing two-component MCR decompositions.

Since the present studies are concerned with interactions between species in three component mixtures containing water, ions, and TBA, it might seem that a three-component MCR algorithm would be required to decompose the measured spectra into contributions arising from each component. We have previously demonstrated that such three-component analyses (performed using MCR-ALS) can be used to

extract SC spectra from reactive mixtures (such as acid–base equilibria).[7] However, in the present studies we have found that it is difficult to obtain reliable three-component MCR-ALS results, presumably because the OH stretch features that are correlated with each of the three components are all highly overlapped. Instead, we have found that more reliable results are produced when using two-component SMCR to analyze spectra obtained by varying one component concentration at a time. For example, if only the alcohol concentration is varied, while holding the salt concentration constant, then the three component mixture is reduced to an effective two-component mixture in which the solvent is a salt solution, and thus the resulting SC spectrum contains features arising from the hydration-shell of the alcohol in the corresponding salt solution. On the other hand, if the alcohol concentration is held constant and the salt concentration is varied, then the resulting SC spectra contain features arising from the hydration-shell of the ions, and thus may include features arising from both water and alcohol molecules which are perturbed by the ions. Both of the latter two-component analysis strategies have proved to be useful in the present studies, as they each provide different information pertaining the interactions between ions and TBA.

All of the Raman spectroscopic measurements described in this work were performed as described previously,[6] with the following exceptions. The power of the 514.5 nm Ar-ion laser was ~50 mW and the integration time for each spectrum was 5 min. Two replicate spectra were collected from each sample and both were used in the MCR analysis of similar pairs of spectra obtained from solutions in which the concentration of one of the components is varied. The measurements were carried out using 1200 gr/mm grating, which produces a dispersion of approximately 1 cm^{-1} per pixel in the OH Raman band spectral region. Raman peak positions were obtained with an accuracy of better than ± 0.5 cm^{-1} by fitting the region near the top of the peak of interest to a Gaussian function.

Fig. 1 contains results which illustrate how Raman-MCR works when applied to salt-free mixtures containing only TBA and water, with either unpolarized (V+H) or depolarized (H) input Raman spectra. Fig. 1A shows the unpolarized Raman spectra of pure water and a 0.5 M aqueous TBA solution. The most obvious difference between these spectra is the presence of the CH stretch bands between 2850 cm^{-1} and 3000 cm^{-1}. These spectra (including replicate measurements) were analyzed using SMCR to obtain the pure water and SC components corresponding to the solid curves in Fig. 1B. Essentially identical results are obtained using MCR-ALS, as well as when using input solution spectra with several different TBA concentrations between 0.1 M and 0.5 M.[7] The dashed curve in Fig. 1B shows depolarized SC spectra (obtained from depolarized input Raman spectra of water and 0.5 M TBA). The difference between the solid and dashed SC curves in Fig. 1B indicates that the lower frequency SC OH stretch (near 3200 cm^{-1}) is more highly polarized than the remaining (higher frequency) SC OH features. Previous theoretical studies of the polarized Raman spectra of pure water have found that highly tetrahedral water structures give rise to strongly polarized low frequency OH stretch Raman scattering.[25–27] Thus, the appearance of a highly polarized low frequency band in the SC spectrum of the hydration-shell of TBA strongly suggests that there is greater tetrahedral order in the hydration-shell of TBA than in bulk water (at 20 °C). In other words, if the hydration-shell of TBA had the same degree of tetrahedral order as the surrounding bulk water, then this polarized low frequency OH band would not appear in the SC spectrum of TBA.

The only pre-processing which was done to the input spectra in order to obtain the results shown in Fig. 1 (as well as the other Raman-MCR results described in this work) is to introduce a slight vertical offset to the solution spectra (but not the pure water spectra), so as to obtain properly converged minimum area SC spectra, which do not dip below the baseline at any point, but reach the baseline at some point within the spectral range within which the solvent spectrum has a finite intensity (above the baseline).

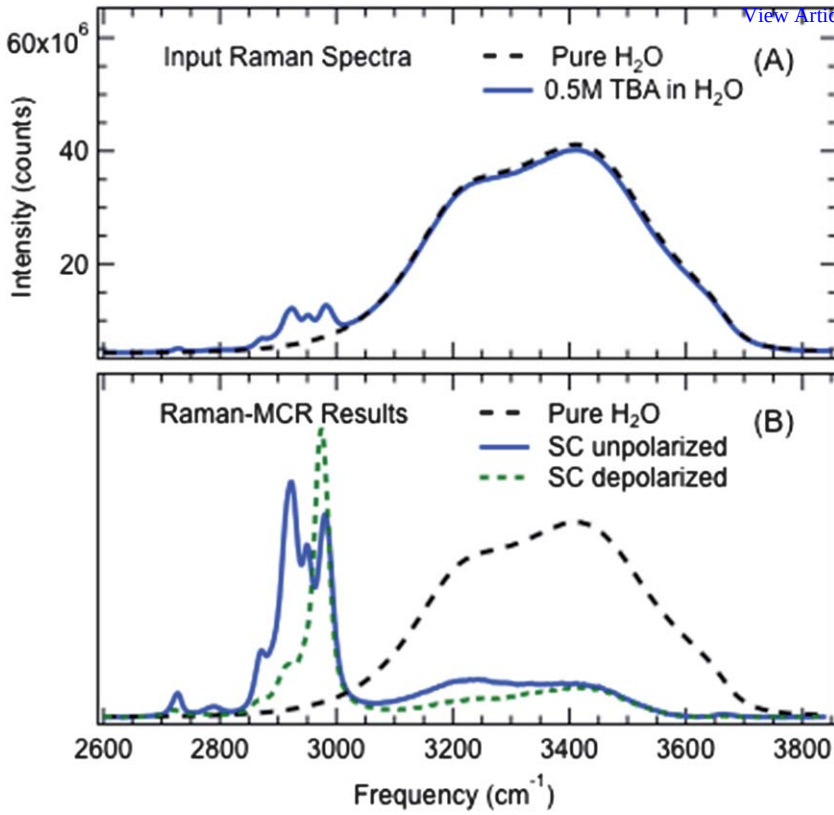

Fig. 1 (A) The input Raman spectra of pure water and 0.5 M TBA in water are compared with (B) the pure water and both the unpolarized and depolarized TBA solute-correlated (SC) spectra obtained using SMCR. The intensities of the spectra in (A) represent the number of counts obtained at each CCD pixel in 5 min of signal averaging, using a 50 mW 514.5 nm excitation laser. The two SC curves in (B) are scaled to the same amplitude in the high frequency region (and the pure water component is scaled to approximately the same height as the SC spectra).

B Theoretical methods and computational details

Water–TBA–ion mixtures were simulated with the general effective fragment potential (EFP) method[8–11] and with the hybrid QM/EFP1 approach. EFP is a quantum mechanics based potential that provides a computationally inexpensive way of modeling intermolecular interactions in non-covalently bound systems. General EFP (originally called EFP2) has four interaction terms, each of which may be thought of as a truncated expansion: Coulomb (electrostatic), induction (polarization), exchange repulsion, and dispersion. An optional charge-transfer term has also been developed.[28] The original implementation of EFP (called EFP1) was specifically designed for describing interactions in water.[8,9,29]

Previously, EFP has been successfully applied for investigation of the non-covalent interactions in small molecular clusters for which EFP was shown to provide accurate results as compared to *ab initio* methods.[30–36] Recently, we employed general EFP to characterize structure and hydrogen bonding in water–TBA solutions.[37] EFP has also been a very useful tool in hybrid quantum mechanics QM/EFP investigations of chemical reactions and solvatochromic effects.[38–46]

EFP implementation has been described elsewhere;[8–11] here we provide computational details specific to the present study. Molecular dynamics (MD)

simulations of water–TBA–ion mixtures were performed with general EFP composed of Coulomb, polarization, dispersion, and exchange-repulsion terms. To account for short-range charge-penetration effects and avoid polarization collapse, Coulomb, polarization, and dispersion interactions were moderated by screening terms.[47–49] Overlap-based electrostatic and dispersion screenings and Gaussian-type polarization screening functions were employed. The polarization screening parameter for Na^+ and I^- ions was set to 0.1; it was kept at a default value of 0.6 for F^-, water, and TBA. Effective potentials for water, TBA, and ions were constructed using the mixed-basis approach, as previously described.[37] Water and TBA potentials were the same as those used previously;[37] multipoles for the Coulomb term were obtained in the 6-31+G* basis,[50–52] while the 6-311++G(3df,2p) basis[53,54] was used for the other terms in water and TBA potentials. 6-31+G* and aug-cc-pVQZ[55,56] basis sets were used for preparing ion potentials.

MD simulations on systems containing 1 TBA molecule, 5 halide and 5 Na^+ ions, and 100 water molecules were performed in a periodic cubic box with dimensions of 14.5 Å and 15.5 Å for F^- and I^- containing mixtures, respectively (corresponding to ~0.55 M TBA added to ~2.7 M aqueous salt solutions). After 10 ps equilibration, five independent 60 ps production runs for NaI solutions and five 100 ps runs for NaF solutions were performed. The results of the independent simulations were averaged. At long range, Coulomb interactions were treated with Ewald summations for charge–charge, charge–dipole, charge–quadrupole, and dipole–dipole terms. Switching functions were employed for other EFP terms.[57] The equations of motion were integrated using the velocity Verlet algorithm with a time step of 0.5 fs. Simulations were performed in the NVT ensemble at 300 K; the temperature was maintained constant using the Nosé–Hoover chain algorithm.

Radial distribution functions (RDF) and angular distributions of ions near TBA and statistics of the water orientations around TBA were gathered from these MD simulations. Additionally, 100 snapshots (collected at random) were sampled for QM/EFP frequency calculations.

The following strategy was employed for evaluating frequency shifts of the CH stretching vibrations of TBA due to the presence of iodide. Sampled structures from EFP/MD simulations were prepared such that TBA was placed in the middle of the simulation box, surrounded by water and ions. Periodic boundary conditions were switched off. The TBA frequencies were calculated using QM/EFP1 and the partial Hessian approach. That is, TBA and ions were comprised in the quantum part and described with the second-order Møller–Plesset perturbation theory using the 6-311++G**[53,54] basis set for TBA and the Hay–Wadt effective core potential for ions.[58] Waters were described by EFP1 water potential. Since only the first derivatives (gradients) are available analytically for QM/EFP1, the second derivatives were calculated numerically. Namely, the Hessian matrix for TBA normal modes was constructed through a set of independent QM/EFP1 gradient calculations with TBA coordinates shifted in both positive and negative directions by 0.005 Å along each x, y, z direction. Positions of ions and waters were kept fixed in these calculations. Vibrational frequencies of TBA were obtained though diagonalization of this partial Hessian matrix. The accuracy of this procedure was tested on small water–TBA clusters by comparing full quantum and partial Hessian QM/EFP1 approaches. Discrepancies in TBA frequencies did not exceed 1 cm^{-1}. To estimate TBA frequency shifts due to a presence of iodide, the averaged TBA frequencies in a pure (salt-free) TBA–water solution were compared to averaged TBA frequencies with iodide ions present. Calculations on 10 structures were performed for averaging the pure-water TBA frequencies and 100 snapshots were used for averaging the frequencies in salt solutions. For salt solutions, separate statistics were gathered for randomly selected snapshots (evenly distributed along MD trajectories) and for the snapshots that contained I^- in the first hydration shell of TBA.

Additionally to liquid calculations, full quantum computations on TBA–water and TBA–I^- dimers were performed. Optimized structures and vibrational frequencies of these clusters were obtained at the MP2/6-311++G** level of theory.

All calculations were performed in the GAMESS electronic structure package.[59,60]

3 Results and discussion

A Aqueous TBA in NaF control experiments

We have performed measurements of TBA in NaF solutions as control experiments, to see if our results confirm that these ions do not significantly interact with TBA. Note that NaF has a maximum aqueous solubility near 1 M, and so that is the highest salt concentration which could be used in these experiments.

Fig. 2 shows the Raman spectra collected from three aqueous solutions, each of which contain 0.5 M TBA but different concentrations of NaF (ranging from 0 M to 1 M). A separate set of spectra was collected from the same solution with no TBA. The latter spectra look very similar to those in Fig. 2, except that they do not contain the CH stretch features between 2850 cm^{-1} and 3000 cm^{-1}. In order to see whether either Na^+ or F^- have any significant interaction with TBA we have performed an SMCR analysis of the spectra obtained at each salt concentration (with and without TBA), just as was done to obtain the salt-free results in Fig. 1.

The resulting SC spectra of TBA, which are shown in Fig. 3, clearly indicate that there is little interaction between NaF and TBA. More specifically, SC spectra in Fig. 3A show no evidence of any significant change in the H-bonded OH hydration-shell features, except for a small (but reproducible) change in the water dangling OH band area (as further discussed in section 3C, below). Similarly, the CH stretch shift results in Fig. 3B show that NaF has no measurable effect on the CH stretch frequency of TBA up to ~1 M NaF. Thus, these results are consistent with the expectation that neither Na^+ nor F^- have any significant affinity for TBA. However, the small change in the dangling OH intensity in the hydration-shell of TBA suggests that the ions in the second or third hydration shell of TBA may slightly influence the structure of TBA's first hydration-shell (as further discussed in Section 3C).

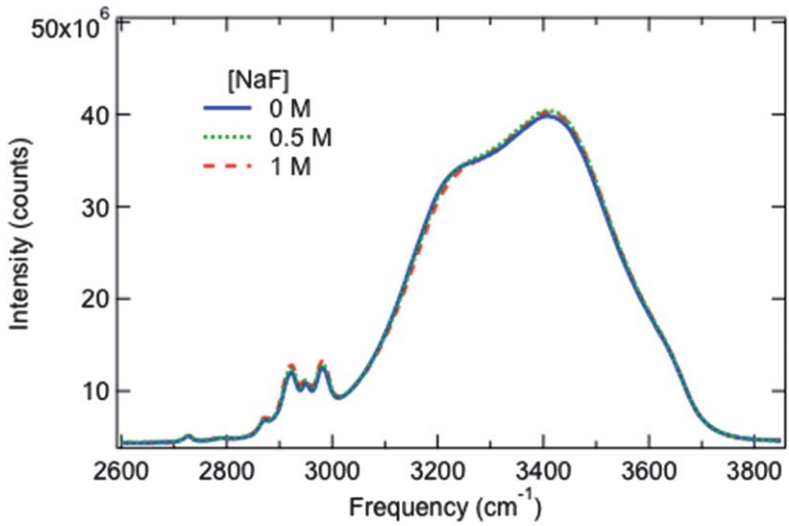

Fig. 2 Raman spectra of water containing 0.5 M TBA and NaF concentrations of either 0 M, 0.5 M or 1 M. The spectra are obtained as described in Fig. 1.

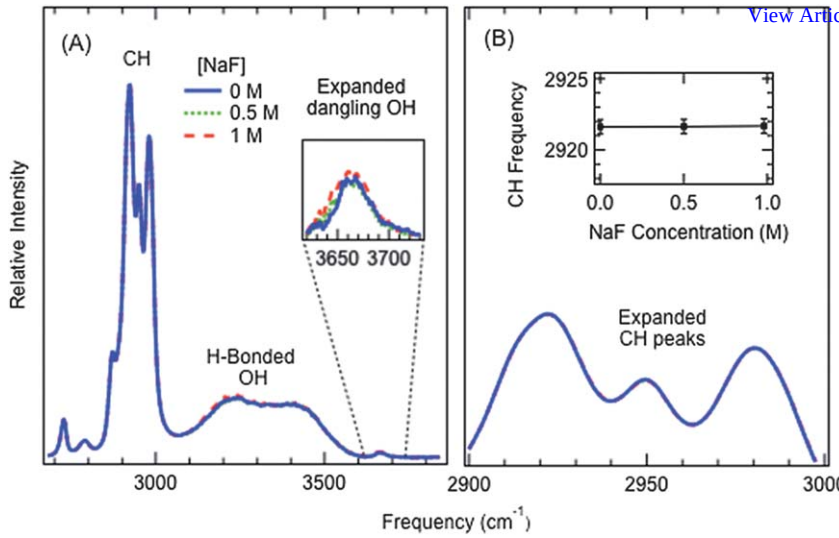

Fig. 3 TBA solute-correlated (SC) spectra obtained from the input spectra shown in Fig. 2 (as well as replicate measurements) in solutions with three different NaF concentrations (0 M, 0.5 M, and 1 M). These SC spectra were each obtained using an independent two-component SMCR analysis of the spectra measured at each salt concentration (with and without TBA).

B Influence of ions on the TBA hydration-shell tetrahedral order

Fig. 4 shows Raman spectra collected from five aqueous solutions, each with ~0.5 M TBA but different concentrations of NaI (ranging from 0 M to 3 M). A separate set of five spectra was collected from the same salt solutions with no TBA. The latter spectra again look quite similar to those in Fig. 4, except that they do not contain the CH stretch features between 2850 cm^{-1} and 3000 cm^{-1}. The change in shape (and increase in intensity) of the OH stretch band with increasing salt concentration is due primarily to H-bonding between water and I^- (and the associated increase in the water OH Raman cross-section) as previously discussed.[4,61] Our present interest

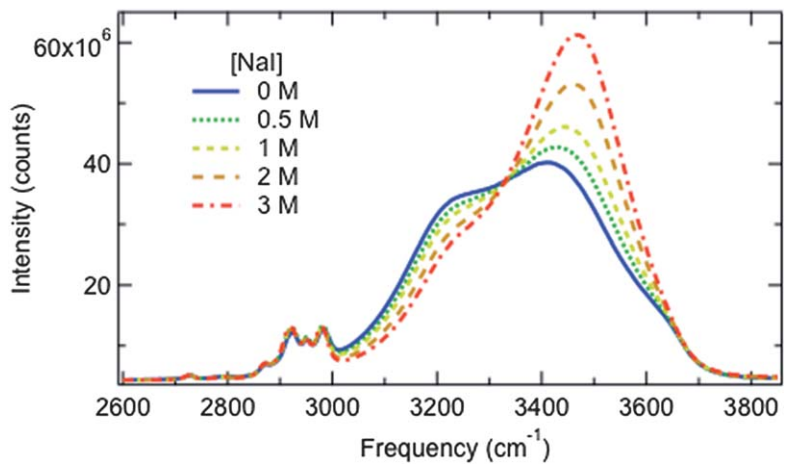

Fig. 4 Raman spectra of aqueous solutions containing 0.5 M TBA and various concentrations of NaI (as indicated in the legend) at 20 °C. The spectra are obtained as described in Fig. 1.

is in elucidating how I^- influences the hydration-shell of TBA, using SC obtained in the same way as was done to get the results in Fig. 1 and 3, by independently analyzing the Raman spectra obtained at each salt concentration (with and without TBA).

The resulting SC spectra of TBA in NaI solutions of various concentrations are shown in Fig. 5A. Note that all of the features in these spectra are correlated with the concentration of TBA and thus include the TBA CH stretch band as well as OH features arising from water molecules in the hydration-shell of TBA. The latter OH features would only appear in the SC spectrum if they differed from the spectra of water molecules in the corresponding salt solution (or pure water). Note that the NaF results shown in Fig. 3 imply that Na^+ cannot be the source of the perturbations that are evidenced in Fig. 5. Thus, any salt concentration dependent changes in the SC spectra shown in Fig. 5 reveal the influence of I^- ions on TBA or its hydration-shell.

Our previous studies have confirmed that alcohol OH head groups contribute very little to hydration-shell OH spectra as, for example, benzene and phenol have virtually identical SC spectra.[6] Thus, the H-bonded OH features in the SC spectra in Fig. 5A (as well as Fig. 1 and 3) arise primarily from water molecules in the hydrophobic hydration shell of TBA.

The most evident effect of NaI on the SC spectrum of TBA is the change in the H-bonded OH stretch features shown in Fig. 5A. Increasing the concentration of NaI clearly leads to a decrease in the intensity of the lower frequency H-bonded OH band, near 3200 cm^{-1}. Since the latter highly polarized Raman band is assigned to water molecules with a high degree of tetrahedral order (as discussed in Section 2), the observed decrease in the area of that low frequency band implies the I^- disrupts the tetrahedral order of the TBA hydration shell (relative to TBA in pure water).

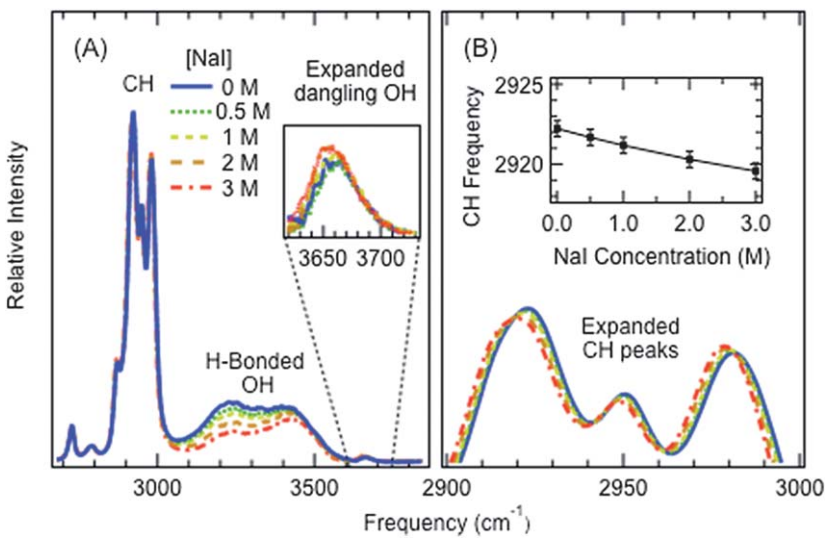

Fig. 5 Solute-correlated (SC) spectra of TBA obtained in solvents with different NaI concentrations. The SC spectra have all been normalized to the same TBA CH band area, so as to compare properly the relative intensities of the corresponding hydration-shell features. Panel (A) shows the full TBA SC spectrum in the CH/OH stretch region, which reveals salt concentration dependent changes in the H-bonded OH region, as well as small salt concentration dependent changes in the intensity of the water dangling OH in the TBA hydration-shell. Panel (B) shows an expanded view of the TBA CH stretch peaks, to reveal that NaI produces a small red-shift in the TBA CH stretch, with a nearly linear NaI concentration dependence (and a slope of $\sim$1 cm^{-1} M^{-1}).

C Influence of ions on the TBA hydration-shell dangling OH bonds

The inserted panel in Fig. 5A shows an expanded view of the small high frequency dangling OH peak that appears in TBA's hydration-shell. Such water dangling OH features have previously been observed both at macroscopic air–water and oil–water interfaces,[62,63] as well as in the hydration shells of hydrocarbon groups dissolved in water.[5,64] In this work, we are interested in using the water dangling OH band to probe interactions between ions and molecular hydrophobic interfaces. If there were a high probability of finding an I^- ion in contact with the CH_3 groups of TBA, then one might expect that increasing the concentration of I^- would *decrease* the dangling OH population in TBA's hydration-shell. However, our results show no such decrease but rather a small, but reproducible, salt-induced increase in the dangling OH intensity.

The magnitude of the dangling OH increase produced by 1 M NaI is in fact very similar to that which was found in 1 M NaF (as shown in Fig. 3A), suggesting that both I^- and F^- produce a slight increase in the number of dangling bonds in the hydration shell of TBA. However, an intensity increase can in general either arise from an increase in population or from an increase in Raman scattering cross-section. Thus, an alternative explanation for the observed dangling OH increase might be that both F^- and I^- increase the Raman cross section of the dangling OH. However, the following argument suggest that the observed dangling bond intensity increase is not due to ion-induced changes in the dangling OH Raman cross section.

Raman spectral results such as those shown in Fig. 4 indicate I^- produces an increase in the Raman cross section of the OH groups to which it is H-bonded,[4,61] and so the other OH group on such water molecules might perhaps also have an enhanced Raman cross section. If that second OH also happened to form one of the dangling OH groups in TBA's hydration shell, then it could contribute the observed intensity increase. However, since F^- *decreases* rather than increases the Raman cross-section of water molecules to which it is H-bonded,[4,61] the above argument would imply that the dangling OH intensity should *decrease* in NaF solutions. Thus, the fact that a similar dangling OH *increase* is found in both NaF and NaI, suggests that the observed intensity increase does not result from anion-induced OH Raman cross section changes, but rather arises from a dangling OH population change.

D Influence of ions on hydrophobic CH vibrational frequencies

The vibrational frequencies of solute CH groups provide another potentially valuable probe of the affinity of ions for molecular hydrophobic hydration-shells. When TBA is dissolved in NaF solutions the resulting SC spectra show essentially no change in the CH stretch frequency of TBA (see Fig. 3B). However, when TBA is dissolved in NaI solutions a small but readily measureable CH red-shift is observed, as shown in Fig. 5B. The approximately linear concentration dependent slope of the latter red-shift has a magnitude of only $\sim$1 cm^{-1} M^{-1}, corresponding to a total shift of $\sim$3 cm^{-1} in a 3 M NaI solution (and all the CH sub-peaks shown in Fig. 5B have comparable shifts). The small magnitude of this red-shift is remarkable given that in a 3 M NaI solution there are fewer than 10 water molecules per ion, and so even random mixing would assure that there would be approximately one I^- in the first hydration shell of every TBA molecule (since there are about $\sim$22 water molecules in the first hydration-shell of TBA).

In order to gauge whether the observed CH frequency shift is consistent with the presence of I^- ions in the first hydration-shell of TBA, we have performed calculations on TBA–water and TBA-I^- dimers as well as TBA dissolved in both liquid water and aqueous NaI. Our dimer MP2/6-311++G** calculations were performed on TBA–water and TBA-I^- dimers in which either water or I^- are situated on the

hydrophobic side of TBA, approximately equally distant from its three CH groups, as shown in Fig. 6. Interestingly, I^- in this hydrophobic hydration-shell location produces a red-shift in the CH frequency of about 20 cm^{-1}, relative to the CH frequency obtained when I^- is replaced by a water molecule. (More specifically, placing a water molecule on the hydrophobic side of TBA produces a *blue*-shift of about 5 cm^{-1} relative to an isolated TBA, while replacing the water by I^- produces a CH *red*-shift of ~15 cm^{-1} relative to an isolated TBA.) The fact that the latter shift is significantly larger that the experimentally observed CH shift (see Fig. 5) might suggest that I^- ions do not significantly occupy the first hydration-shell of TBA. However, the above cluster result may not accurately reflect the predicted shift induced by I^- in hydration-shell of TBA dissolved in aqueous NaI, both because I^- may not be located in the same place as in the above dimers and because the negative charge of I^- may be screened and/or redistributed among surrounding water molecules. Thus, the following liquid simulations were performed in order to more accurately predict the CH frequency shift induced by I^- ions in the first hydration shell of TBA.

Hybrid QM/EFP1 simulations of TBA in pure water and aqueous NaI were performed as described in Section 2B. The resulting TBA CH frequency shifts are shown in Table 1. These TBA frequency shift predictions were obtained using the same level of theory (MP2/6-311++G**) which was used to obtain the above dimer results, while representing water molecules by semi-classical EFP1 potentials. The frequency shifts listed in the fourth column of Table 1 correspond to those obtained for TBA molecules whose first hydration-shell contains an I^- ion. The average value of the red-shift of all the strongly Raman active CH stretch modes is ~4 ± 1 cm^{-1}, which is significantly smaller than the ~20 cm^{-1} red-shift predicted for the gas phase dimers (containing TBA and either water or I^-). Thus, our liquid QM/EFP1 calculations imply that the relatively small magnitude of experimentally observed frequency shift (as shown in Fig. 5) is consistent with the presence of I^- ions in the first hydration shell of TBA (as further discussed below).

The experimental results in Fig. 5 pertain to the CH frequency shift of the total population of TBA molecules in a given salt solution (compared to TBA in pure water). Our simulation results for the total TBA population in aqueous NaI are not sufficiently accurate to determine reliably the corresponding average CH frequency shift, relative to TBA in pure water. More specifically, the average CH frequency of TBA in ~2.7 M NaI was found to be within less than 1 cm^{-1} from that of TBA in pure water.

In order to more directly compare the predictions in Table 1 with experimental measurements, as well as to experimentally estimate the concentration of I^- in the first hydration-shell of TBA, we have used the following alternative two-component SMCR analysis strategy. This was done by collecting Raman spectra of 0.5 M TBA solutions to which various amounts of NaI were added. The resulting I^- SC spectra,

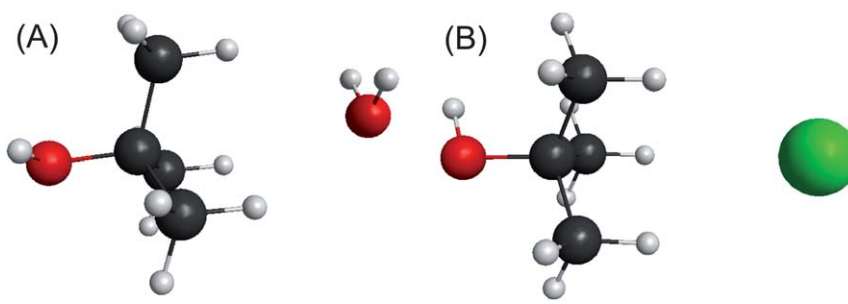

Fig. 6 Local minimum energy structures of TBA–water and TBA-I^- clusters.

Table 1 Predicted TBA CH stretch frequencies (cm^{-1}) and shifts in a ~2.7 M aqueous NaI solution (with respect to the TBA frequencies in pure water, so negative values correspond to red shifts)

TBA in pure water			I^- in the first hydration shell	
CH Frequency	σ^a	Strongly Raman active[b]	Shift[c]	σ^a
3110.4	±1.9	no	−5.71	±1.06
3114.9	±2.2	yes	−5.01	±0.96
3124.1	±2.4	yes	−4.00	±1.40
3199.4	±2.3	no	−7.88	±1.46
3205.6	±2.8	yes	−6.11	±1.12
3216.6	±1.6	yes	−2.20	±1.23
3221.3	±1.8	no	−2.50	±1.01
3224.9	±2.1	yes	−2.18	±0.96
3230.9	±4.8	yes	−2.14	±2.77
Mean frequency shift[c]			−4	±1

[a] Standard deviation of the average frequency of a mode in pure water. [b] Raman activity based on gas phase and TBA–water dimer calculations. [c] CH frequency shift, relative to TBA in pure water. The mean frequency shift (on the bottom row) is obtained from the average of the strongly Raman active CH stretch frequency shifts.

obtained using SMCR, necessarily contain features arising from the hydration-shell of the I^- ions. Previous Raman-MCR studies of aqueous solutions of various alkali-halides have shown that the OH stretch spectra of water are primarily influenced by the anion to which water is directly H-bonded. In the present three component systems, we expect the I^- SC spectrum to contain both features arising from water molecules that are H-bonded to I^-, as well as features arising from the sub-population of TBA molecules that are strongly perturbed by I^-.

Fig. 7 shows Raman-MCR results obtained by adding various concentrations of NaI to a "solvent" composed of 0.5 M aqueous TBA. The spectra shown in Fig. 7 pertain to a mixture containing 3 M NaI (and 0.5 M TBA); the blue curve is the aqueous TBA "solvent" component, while the red curve is the I^- SC spectrum. The higher frequency H-bonded OH stretch band in the red SC spectrum is virtually identical to that previously obtained from solutions of NaI in water (with no TBA), and thus pertains to water OH groups that are H-bonded to I^-. The more interesting feature in the spectra shown in Fig. 7 is the CH band which appears in both the aqueous TBA solvent and I^- SC spectra. The fact that this band appears in the I^- SC spectrum implies that it arises from TBA molecules which are strongly perturbed by I^-. The frequency of the SC CH stretch is red-shifted by $\sim 5 \pm 0.5$ cm^{-1} relative to the CH stretch of TBA in pure water. The latter frequency shift is very close to the $\sim 4 \pm 1$ cm^{-1} red-shift shown in Table 1, which was obtained from the liquid QM/EFP1 simulations for TBA molecules whose first hydration-shells contain an I^- ion.

The relative areas of the CH bands in Fig. 7 may further be used to estimate the number of TBA molecules which are strongly perturbed by I^-. More specifically, the relative area of the CH band in the SC (solid) and total (dashed) curves implies that about 64% of the TBA molecules in a 3 M NaI solution are strongly perturbed by I^-. However, a fundamental "rotational ambiguity" associated with MCR[7] implies that minimum area SC spectra (such as those obtained in this work) have areas which represent a *lower bound* to the true SC spectrum. Thus, although it is possible that only 64% of the TBA molecules are perturbed by I^- it is also possible that some larger fraction of TBA molecules are (less strongly) perturbed by I^-. If we assume that 64% is the actual number of TBA molecules whose first hydration shells contain

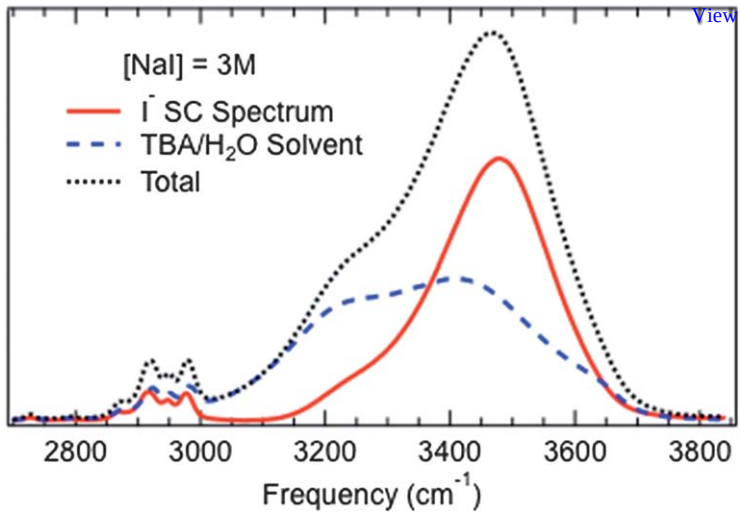

Fig. 7 Raman-MCR is used to decompose the measured spectrum of a solution containing 0.5 M TBA and 3 M NaI (dotted curve) into aqueous TBA (dashed curve) and I^- SC (solid curve) components. The frequency and area differences between the CH bands in the red and blue spectra may be used to quantify the average I^- induced CH frequency shift of the TBA molecules that are strongly perturbed by I^- as well as the number of such strongly perturbed TBA molecules.

one iodide, that would imply that the local concentration I^- is less than 2 M (and thus is below the 3 M concentration of the surrounding NaI solution). This conclusion is consistent with our EFP/MD liquid simulations which suggest that about 89% of the TBA molecules in a ~2.7 M NaI solution have one I^- ion in their first hydration shell. The latter number includes I^- ions that are in the proximity of the hydroxyl group of TBA (as further explained below).

The radial distribution functions shown in Fig. 8 provide additional information that supports and extends the conclusions reached based on our experimental Raman-MCR measurements. For example, our liquid simulations of TBA in ~2.7 M NaF confirm that F^- is essentially never found in the first hydration shell of TBA, which is consistent with the results shown in Fig. 3, which indicate that NaF has virtually no influence on the hydration shell of TBA or its CH frequency. More importantly, our simulation results are consistent with the experimental finding that there is a significant probability of finding an I^- ion in the first hydration shell of TBA, although the local concentration of I^- is lower than it is in the surrounding bulk, and so I^- is not attracted to the hydration shell of TBA, although it is apparently not repelled from the hydration-shell as much as Na^+ and F^-

Our EFP/MD simulations also provide information pertaining to the angular distribution of I^- ions within TBA's first hydration-shell, as shown in Fig. 9. This angular distribution is normalized such that an isotropic (perfectly spherical) distribution would have a value of 1 at all angles. The distribution shown in the lower curve of Fig. 9, which corresponds to ions found within 6.5 Å from the central carbon atom of TBA (near the minimum in TBA–water RDF, see Fig. 8), implies that the I^- ions are most likely to be located in the regions of ~0°–20°, ~30°–70°, ~80°–140°, or near 180°. Angles greater that ~80° correspond to I^- ions located around the periphery of TBA's CH_3 groups, while smaller angles correspond to ions interacting with the OH head group of TBA. The peak at ~30°–70° is consistent with I^- ions H-bonded to the OH head group of TBA. The peak at ~0°–20° completely disappears in the angular distribution pertaining to the shorter (5.3 Å) C_{TBA}-I^- cut-off distance (see Fig. 9, upper curve). This means that I^- ions in this angular range are located between 5.3 Å and 6.5 Å from central TBA carbon; a

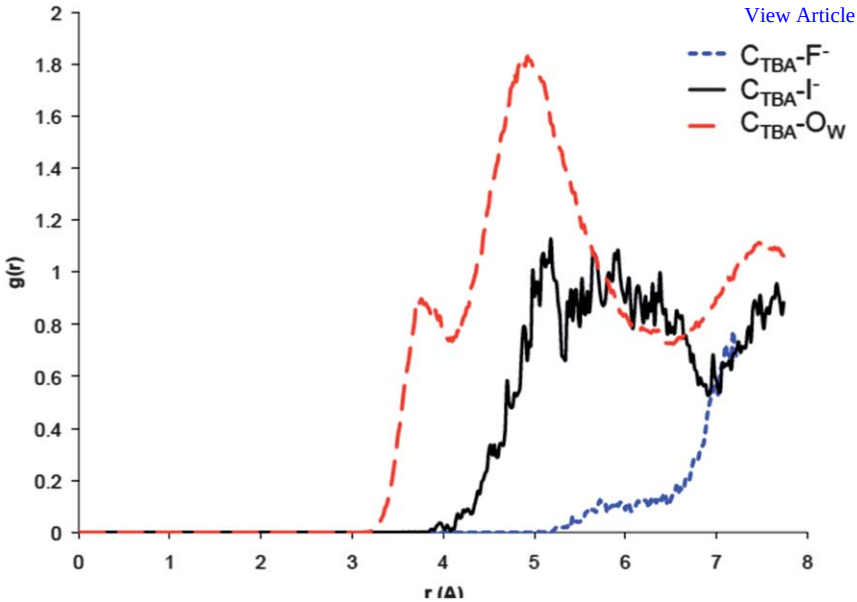

Fig. 8 Radial distribution functions between the central carbon in TBA and F^- (dotted curve), I^- (solid curve), and water oxygen (dashed curve). The first maximum in the TBA-I^- RDF at ~5.1 Å corresponds to ions directly in contact with TBA; the second broader peak extending out to ~6.5 Å includes ions that are interacting with a water molecule that is H-bonded to the TBA OH head group.

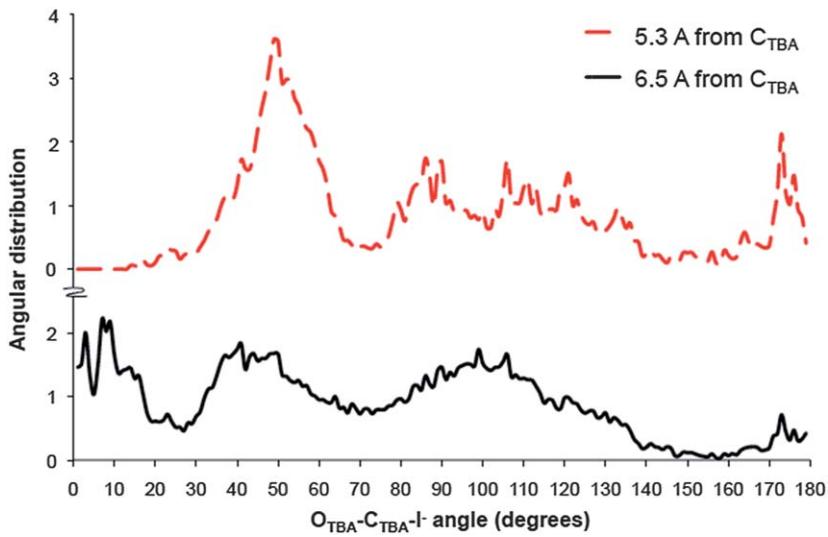

Fig. 9 The angular distribution of I^- ions within TBA's first hydration shell is normalized such that a perfectly isotropic distribution would have a value of 1 at all angles. At angles greater than 80° the ion is on the hydrophobic side of TBA. The upper (dashed) curve corresponds to ions that are within 5.3 Å of the central carbon atom of TBA. The lower (solid) curve corresponds to ions that are within 6.5 Å of the central carbon atom of TBA.

detailed investigation of the corresponding snapshots shows that these ions are bridged by a water molecule H-bonded to the OH head group of TBA.

4 Conclusions

We have combined experimental (Raman-MCR) measurements with theoretical cluster and liquid (EFP/MD) calculations to probe quantitatively and compare the affinities of F^- and I^- for the first hydration-shell of t-butyl alcohol (TBA). Our results indicate that while F^- (as well as Na^+) is strongly excluded from the first hydration shell of TBA, the local concentration of I^- around TBA is nearly as large as the surrounding bulk NaI concentration. The latter conclusion is supported by our experimental findings that in ~3 M NaI approximately two thirds of the TBA molecules are strongly perturbed by I^-, and those strongly perturbed TBA molecules have a CH stretch Raman frequency which is red-shifted by ~5 cm^{-1} relative to TBA in pure water. Both of the latter experimental observations are in good agreement with our theoretical EFP/MD and QM/EFP1 predictions. Our liquid simulation results further indicate that I^- ions are most likely to be located either near TBA's head group or around the periphery of its CH_3 groups, rather than up against the hydrophobic end of TBA. We have further found experimental evidence that I^- disrupts the tetrahedral order in the hydration shell of TBA and that both F^- and I^- slightly increase the intensity of the narrow high-frequency dangling OH peak in the hydration-shell spectrum of TBA. The latter dangling OH intensity increase is not likely to be due to an anion-induced Raman cross section change (as F^- and I^- have opposite effects on the OH cross section of water), but may indicate that the probability that water will form a dangling OH bond around TBA is increased by ions in the second (or higher) hydration shell(s) of TBA.

Acknowledgements

The work done by D. B. A., B. M. R., and D. W. was supported by a grant from the National Science foundation (CHE-0847928), while that done by L. V. S. and M. D. H. was supported by a CAREER grant from the National Science foundation (grant CHE-0955419) and Purdue University. We thank Ben Nebgen for help in preparing a script for performing semi-numerical frequency calculations, and Joe Thomaz for performing MCR-ALS three component analyses to compare with the SMCR results reported in this work.

References

1 Y. Levin, A. P. dos Santos and A. Diehl, *Phys. Rev. Lett.*, 2009, **103**(257802), 257801–257804.
2 W. Kunz, P. Lo Nostro and B. W. Ninham, *Curr. Opin. Colloid Interface Sci.*, 2004, **9**, 1–18.
3 P. Perera, M. Wyche, Y. Loethen and D. Ben-Amotz, *J. Am. Chem. Soc.*, 2008, **130**, 4576–4579.
4 P. N. Perera, B. Browder and D. Ben-Amotz, *J. Phys. Chem. B*, 2009, **113**, 1805–1809.
5 P. N. Perera, K. R. Fega, C. Lawrence, E. J. Sundstrom, J. Tomlinson-Phillips and D. Ben-Amotz, *Proc. Natl. Acad. Sci. U. S. A.*, 2009, **106**, 12230–12234.
6 K. P. Gierszal, J. G. Davis, M. D. Hands, D. S. Wilcox, L. V. Slipchenko and D. Ben-Amotz, *J. Phys. Chem. Lett.*, 2011, **2**, 2930–2933.
7 K. R. Fega, D. S. Wilcox and D. Ben-Amotz, *Appl. Spectrosc.*, 2011, **66**, 282–288.
8 P. N. Day, J. H. Jensen, M. S. Gordon, S. P. Webb, W. J. Stevens, M. Krauss, D. Garmer, H. Basch and D. Cohen, *J. Chem. Phys.*, 1996, **105**, 1968–1986.
9 M. S. Gordon, M. A. Freitag, P. Bandyopadhyay, J. H. Jensen, V. Kairys and W. J. Stevens, *J. Phys. Chem. A*, 2001, **105**, 293–307.
10 M. S. Gordon, L. V. Slipchenko, H. Li and J. H. Jensen, *Annu. Rep. Comput. Chem.*, 2007, **3**, 177–193.

11 D. Ghosh, D. Kosenkov, V. Vanovschi, C. F. Williams, J. M. Herbert, M. S. Gordon, M. W. Schmidt, L. V. Slipchenko and A. I. Krylov, *J. Phys. Chem. A*, 2010, **114**, 12739–12754.
12 J. Cheng, M. R. Hoffmann and A. J. Colussi, *J. Phys. Chem. B*, 2008, **112**, 7157–7161.
13 S. Ghosal, J. C. Hemminger, H. Bluhm, B. S. Mun, E. L. D. Hebenstreit, G. Ketteler, D. F. Ogletree, F. G. Requejo and M. Salmeron, *Science*, 2005, **307**, 563–566.
14 V. Padmanabhan, J. Daillant, L. Belloni, S. Mora, M. Alba and O. Konovalov, *Phys. Rev. Lett.*, 2007, **99**(086105), 086101–086104.
15 H. C. Allen, N. N. Casillas-Ituarte, M. R. Sierra-Hernandez, X. K. Chen and C. Y. Tang, *Phys. Chem. Chem. Phys.*, 2009, **11**, 5538–5549.
16 P. B. Petersen and R. J. Saykally, *J. Am. Chem. Soc.*, 2005, **127**, 15446–15452.
17 J. K. Beattie, P. Creux and A. Gray-Weale, *Aust. J. Chem.*, 2011, **64**, 1580–1582.
18 B. L. Eggimann and J. I. Siepmann, *J. Phys. Chem. C*, 2008, **112**, 210–218.
19 D. Horinek, A. Herz, L. Vrbka, F. Sedlmeier, S. I. Mamatkulov and R. R. Netz, *Chem. Phys. Lett.*, 2009, **479**, 173–183.
20 B. A. Bauer, S. C. Ou and S. Patel, *Chem. Phys. Lett.*, 2012, **527**, 22–26.
21 P. Jungwirth and D. J. Tobias, *Chem. Rev.*, 2006, **106**, 1259–1281.
22 (*a*) P. Jungwirth, *Faraday Discuss.*, 2009, **141**, 9–30; (*b*) K. B. Rembert, J. Paterová, J. Heyda, C. Hilty, P Jungwirth and P. S. Cremer, *J. Am. Chem. Soc.*, 2012, **134**, 10039–10046.
23 M. D. Baer and C. J. Mundy, *J. Phys. Chem. Lett.*, 2011, **2**, 1088–1093.
24 W. H. Lawton and E. A. Sylvestre, *Technometrics*, 1971, **13**, 617–633.
25 H. Torii, *J. Phys. Chem. A*, 2006, **110**, 9469–9477.
26 M. Yang and J. L. Skinner, *Phys. Chem. Chem. Phys.*, 2010, **12**, 982–991.
27 B. M. Auer and J. L. Skinner, *Chem. Phys. Lett.*, 2009, **470**, 13–20.
28 H. Li, M. S. Gordon and J. H. Jensen, *J. Chem. Phys.*, 2006, **124**, 214108.
29 I. Adamovic, M. A. Freitag and M. S. Gordon, *J. Chem. Phys.*, 2003, **118**, 6725–6732.
30 P. N. Day, R. Pachter, M. S. Gordon and G. N. Merrill, *J. Chem. Phys.*, 2000, **112**, 2063–2073.
31 I. Adamovic and M. S. Gordon, *J. Phys. Chem. A*, 2006, **110**, 10267–10273.
32 I. Adamovic, H. Li, M. H. Lamm and M. S. Gordon, *J. Phys. Chem. A*, 2006, **110**, 519–525.
33 T. Smith, L. V. Slipchenko and M. S. Gordon, *J. Phys. Chem. A*, 2008, **112**, 5286–5294.
34 Q. A. Smith, M. S. Gordon and L. V. Slipchenko, *J. Phys. Chem. A*, 2011, **115**, 4598–4609.
35 Q. A. Smith, M. S. Gordon and L. V. Slipchenko, *J. Phys. Chem. A*, 2011, **115**, 11269–11276.
36 L. V. Slipchenko and M. S. Gordon, *J. Phys. Chem. A*, 2009, **113**, 2092–2102.
37 M. D. Hands and L. V. Slipchenko, *J. Phys. Chem. B*, 2012, **116**, 2775–2786.
38 J. M. Mullin and M. S. Gordon, *J. Phys. Chem. B*, 2009, **113**, 8657–8669.
39 J. M. Mullin and M. S. Gordon, *J. Phys. Chem. B*, 2009, **113**, 14413–14420.
40 D. Kosenkov and L. V. Slipchenko, *J. Phys. Chem. A*, 2011, **115**, 392–401.
41 L. V. Slipchenko, *J. Phys. Chem. A*, 2010, **114**, 8824–8830.
42 A. DeFusco, N. Minezawa, L. V. Slipchenko, F. Zahariev and M. S. Gordon, *J. Phys. Chem. Lett.*, 2011, **2**, 2184–2192.
43 D. Ghosh, O. Isayev, L. V. Slipchenko and A. I. Krylov, *J. Phys. Chem. A*, 2011, **115**, 6028–6038.
44 S. P. Webb and M. S. Gordon, *J. Phys. Chem. A*, 1999, **103**, 1265–1273.
45 I. Adamovic and M. S. Gordon, *J. Phys. Chem. A*, 2005, **109**, 1629–1636.
46 S. Yoo, F. Zahariev, S. Sok and M. S. Gordon, *J. Chem. Phys.*, 2008, **129**, 144112–144118.
47 M. A. Freitag, M. S. Gordon, J. H. Jensen and W. J. Stevens, *J. Chem. Phys.*, 2000, **112**, 7300–7306.
48 L. V. Slipchenko and M. S. Gordon, *J. Comput. Chem.*, 2007, **28**, 276–291.
49 L. V. Slipchenko and M. S. Gordon, *Mol. Phys.*, 2009, **107**, 999–1016.
50 W. J. Hehre, R. Ditchfield and J. A. Pople, *J. Chem. Phys.*, 1972, **56**, 2257.
51 P. C. Hariharan and J. A. Pople, *Theor. Chim. Acta*, 1973, **28**, 213–222.
52 T. Clark, J. Chandrasekhar, G. W. Spitznagel and P. V. Schleyer, *J. Comput. Chem.*, 1983, **4**, 294–301.
53 R. Krishnan, J. S. Binkley, R. Seeger and J. A. Pople, *J. Chem. Phys.*, 1980, **72**, 650–654.
54 M. J. Frisch, J. A. Pople and J. S. Binkley, *J. Chem. Phys.*, 1984, **80**, 3265–3269.
55 T. H. Dunning, *J. Chem. Phys.*, 1989, **90**, 1007–1023.
56 R. A. Kendall, T. H. Dunning and R. J. Harrison, *J. Chem. Phys.*, 1992, **96**, 6796–6806.
57 H. Li, H. M. Netzloff and M. S. Gordon, *J. Chem. Phys.*, 2006, **125**, 194103.
58 W. R. Wadt and P. J. Hay, *J. Chem. Phys.*, 1985, **82**, 284–298.
59 M. W. Schmidt, K. K. Baldridge, J. A. Boatz, S. T. Elbert, M. S. Gordon, J. H. Jensen, S. Koseki, N. Matsunaga, K. A. Nguyen, S. J. Su, T. L. Windus, M. Dupuis and J. A. Montgomery, *J. Comput. Chem.*, 1993, **14**, 1347–1363.

60 M. S. Gordon and M. W. Schmidt, in *Theory and Applications of Computational Chemistry*, ed. C. E. Dykstra, G. Frenking, K. S. Kim and G. E. Scuseria, Elsevier, 2005, ch. 41.
61 J. D. Smith, R. J. Saykally and P. L. Geissler, *J. Am. Chem. Soc.*, 2007, **129**, 13847–13856.
62 Q. Du, E. Freysz and Y. R. Shen, *Science*, 1994, **264**, 826–828.
63 F. G. Moore and G. L. Richmond, *Acc. Chem. Res.*, 2008, **41**, 739–748.
64 J. Tomlinson-Phillips, J. Davis, D. Ben-Amotz, D. Spangberg, L. Pejov and K. Hermansson, *J. Phys. Chem. A*, 2011, **115**, 6177–6183.

